

A Numerical Study of the Light Bullets Interaction in the (2+1) Sine-Gordon Equation

T. Povich¹ and J. Xin²

¹ Department of Mathematical Sciences, United States Military Academy, West Point, NY
10996, USA

e-mail: at9970@usma.edu

² Department of Mathematics and ICES, University of Texas at Austin, Austin, TX 78712,
USA

e-mail: jxin@math.utexas.edu

Received June 13, 2003; accepted October 19, 2004.

Online publication March 11, 2005.

Communicated by M. I. Weinstein.

Summary. The propagation and interaction in more than one space dimension of localized pulse solutions (so-called light bullets) to the sine-Gordon [SG] equation is studied both asymptotically and numerically. Similar solutions and their resemblance to solitons in integrable systems were observed numerically before in vector Maxwell systems. The simplicity of SG allows us to perform an asymptotic analysis of counterpropagating pulses, as well as a fully resolved computation over rectangular domains. Numerical experiments are carried out on single pulse propagation and on two pulse collision under different orientations. The particle nature, as known for solitons, persists in these two space dimensional solutions as long as the amplitudes of initial data range in a finite interval, similar to the conditions on the vector Maxwell systems.

1. Introduction

Spatially localized propagating waves (pulses) with particle features in more than one space dimension are of both physical and mathematical interest. They form an extension of the well-known one space dimensional solitons [1]. Recently in nonlinear optics, such waves have been computed numerically as solutions to the classical Maxwell systems with cubic nonlinearities, and have been called light bullets [LB] [2]. LBs have been found to be useful as information carriers in communication and as energy sources, and have also been proposed for the design of optical switches and logic gates in future all-optical devices [3].

Mathematically, one faces new challenges as well. The higher space-dimensional nonlinear wave equations are usually not integrable. This motivates one to study simpler

nonlinear wave equations that admit LB-like solutions. The (2+1) sine-Gordon [SG] equation is such a prototype equation. In [9], SG is derived from a cubic nonlinear Maxwell system, and single pulse propagation is asymptotically analyzed and computed.

This paper continues this line of inquiry for colliding (2+1) SG pulses through theory and computation. A slowly varying envelope analysis is performed on counterpropagating pulses, and a coupled system of nonlinear wave equations is derived on the interaction effects. The asymptotic solutions provide a theoretical basis for the robust pulse collision observed later in numerical solutions. Moreover, the asymptotics help to prepare the initial data for computation. It is numerically demonstrated that the LB solutions of the (2+1) SG and their interactions on the plane resemble the Maxwell LBs of [2]. The LB solutions persist in time if the amplitudes of initial data remain in a certain finite range. The persistence is related to the breathing motion of the LB solutions; see [9], [4], [5] for combined asymptotic and numerical studies using different methods. In [4] and [5], radiation effects are analyzed and found to be a stabilizing mechanism.

The rest of the paper is organized as follows. In Section 2, the slowly varying envelope asymptotics (SVEA) is presented on a pair of counterpropagating pulses. Global well-posedness of the derived asymptotic equations is proved by the energy method. In Section 3, after a brief discussion of the numerical method, initial conditions, and numerical parameters, numerical results are reported for four different cases: the single pulse, the axial collision, the 90-degree and 120-degree collisions. Robustness of LBs under parameter variations is also studied. We conclude in Section 4 and discuss future areas of research.

2. Envelope Asymptotics

Consider the initial value problem of the $(n + 1)$ SG equation:

$$u_{tt} - \Delta_x u + \sin u = 0, \quad x = (x_1, x_2, \dots, x_n) \in R^n, \quad (2.1)$$

$n \geq 2$, $(u, u_t)(0, x) \in (H^1(R^n))^2$, where Δ_x is the Laplacian. Let us look for an asymptotic solution containing two counterpropagating pulses along x_1 with slowly varying envelopes:

$$\begin{aligned} u &\sim \epsilon(A^+(\chi^+, \epsilon y, T; \epsilon) + \epsilon B^+(\epsilon x, \tau; \epsilon))e^{i(kx_1 - \omega t)} \\ &\quad + \epsilon(A^-(\chi^-, \epsilon y, T; \epsilon) + \epsilon B^-(\epsilon x, \tau; \epsilon))e^{i(kx_1 + \omega t)} + c.c. + R \\ &\equiv u_A + R, \end{aligned} \quad (2.2)$$

where $x = (x_1, y)$, $\chi^\pm = \epsilon(x_1 \mp vt)$, $(X_1, Y, \tau, T) = (\epsilon x_1, \epsilon y, \epsilon t, \epsilon^2 t)$, $\omega = \sqrt{1 + k^2}$, $v = k/\omega$ (the group velocity), c.c. complex conjugate. The function R is the remainder. The A^\pm terms are similar to those in single pulse asymptotics [9], while the B^\pm terms are there to capture the interactions.

The ansatz (2.2) is an extension of the one in [7] for counterpropagating pulses in the (1+1) sine-Gordon equations by including higher order resonant terms in the expansion so that there is no finite time collapse due to truncation at cubic order. The formal ansatz (2.2) reveals the analytical structure of pulse interactions. However, we do not address the

validity issue, and only use the ansatz for selecting initial data for numerical simulations in later sections.

We substitute the ansatz (2.2) into SG, and separate the linear from nonlinear terms. It follows that

$$\begin{aligned}
0 = & R_{tt} - \Delta_x R + R \\
& + \epsilon^3 e^{i(kx_1 - \omega t)} \left[(-2i\omega) A_T^+ + (v^2 - 1) A_{X^+ X^+}^+ - A_{YY}^+ - 2\epsilon v A_{X^+ T}^+ + \epsilon^2 A_{TT}^+ \right] \\
& + \epsilon^3 e^{i(kx_1 - \omega t)} \left[(-2i\omega) B_\tau^+ - (2ik) B_{X_1}^+ + \epsilon B_{\tau\tau}^+ - \epsilon B_{X_1 X_1}^+ - \epsilon B_{YY}^+ \right] \\
& + \epsilon^3 e^{i(kx_1 + \omega t)} \left[(2i\omega) A_T^- + (v^2 - 1) A_{X^- X^-}^- - A_{YY}^- - 2\epsilon v A_{X^- T}^- + \epsilon^2 A_{TT}^- \right] \\
& + \epsilon^3 e^{i(kx_1 + \omega t)} \left[(2i\omega) B_\tau^- - (2ik) B_{X_1}^- + \epsilon B_{\tau\tau}^- - \epsilon B_{X_1 X_1}^- - \epsilon B_{YY}^- \right] + c.c. \\
& + \sum_{j=1}^{\infty} (-1)^j ((2j+1)!)^{-1} u_A^{2j+1} \\
& + \sum_{j=1}^{\infty} (-1)^j ((2j+1)!)^{-1} [(u_A + R)^{2j+1} - u_A^{2j+1}]. \tag{2.3}
\end{aligned}$$

Now we extract resonant terms (terms multiplied by $e^{i(kx_1 \pm \omega t)}$) from the first infinite sum of (2.3), in which $*$ means taking the complex conjugate:

$$\left(e^{i(kx_1 - \omega t)} \sum_{j \geq 1, (m_1, m_2, n_1, n_2) \in \Sigma_j} + e^{i(kx_1 + \omega t)} \sum_{j \geq 1, (m_1, m_2, n_1, n_2) \in \Gamma_j} \right)$$

$$\begin{aligned}
& C_{m_1, m_2, n_1, n_2}^{2j+1} (A^+ + \epsilon B^+)^{m_1} \cdot (A^{+,*} + \epsilon B^{+,*})^{m_2} \cdot (A^- + \epsilon B^-)^{n_1} \cdot (A^{-,*} + \epsilon B^{-,*})^{n_2} \\
& \cdot \epsilon^{2j+1} (-1)^j \cdot [(2j+1)!]^{-1}, \tag{2.4}
\end{aligned}$$

where $C_{m_1, m_2, n_1, n_2}^{2j+1}$ is the combination number, and Σ_j denotes the resonant modes ($m_i, n_i \geq 0, i = 1, 2$):

$$m_1 + m_2 + n_1 + n_2 = 2j + 1, \tag{2.5}$$

$$m_1 - m_2 + n_1 - n_2 = 1, \tag{2.6}$$

$$-m_1 + m_2 + n_1 - n_2 = -1, \tag{2.7}$$

and Γ_j consists of (2.5)–(2.6) and

$$-m_1 + m_2 + n_1 - n_2 = 1. \tag{2.8}$$

Other resonant modes are not generic (they exist for special ks) and are not included. In particular, if k^2 is irrational, the nongeneric modes do not appear. The first sum in (2.4) without the exponential prefactor will be denoted by $\epsilon^3 N_+(\epsilon(A^+ + \epsilon B^+), \epsilon(A^- + \epsilon B^-))$, and similarly the second sum in (2.4) without the exponential prefactor will be denoted by $\epsilon^3 N_-(\epsilon(A^+ + \epsilon B^+), \epsilon(A^- + \epsilon B^-))$.

The second infinite sum in (2.3) contains terms proportional to R and its higher powers multiplied by powers of u_A . The envelope equations are derived by removing all

the above resonance terms to minimize the growth of the error term R . As the A^\pm only depend on T and χ^\pm , or different characteristic variables, they satisfy separate equations:

$$0 = (-2i\omega)A_T^+ + (v^2 - 1)A_{\chi^+\chi^+}^+ - A_{YY}^+ - 2\epsilon v A_{\chi^+T}^+ + \epsilon^2 A_{TT}^+ + N_0(A^+, \epsilon), \quad (2.9)$$

where

$$N_0(A^+, \epsilon) \equiv \epsilon^{-3} \sum_{j=1}^{\infty} (-1)^j [(j+1)!j!]^{-1} \epsilon^{2j+1} |A^+|^{2j} A^+,$$

and

$$0 = (2i\omega)A_T^- + (v^2 - 1)A_{\chi^-\chi^-}^- - A_{YY}^- - 2\epsilon v A_{\chi^-T}^- + \epsilon^2 A_{TT}^- + N_0(A^-, \epsilon). \quad (2.10)$$

Equations (2.9) and (2.10) are globally well-posed [9] and observed numerically to track evolution of single pulses [10] at small but fixed ϵ . The nonlinearity N_0 is asymptotic to linear growth for large argument A^\pm at any fixed ϵ [9].

The remaining resonance is removed by a coupled wave system on B^\pm :

$$\begin{aligned} 0 = & (-2i\omega) B_\tau^+ - (2ik) B_{X_1}^+ + \epsilon B_{\tau\tau}^+ - \epsilon B_{X_1 X_1}^+ \\ & - \epsilon B_{YY}^+ + N_+(\epsilon(A^+ + \epsilon B^+), \epsilon(A^- + \epsilon B^-)) - N_0(A^+, \epsilon), \end{aligned} \quad (2.11)$$

and

$$\begin{aligned} 0 = & (2i\omega) B_\tau^- - (2ik) B_{X_1}^- + \epsilon B_{\tau\tau}^- - \epsilon B_{X_1 X_1}^- \\ & - \epsilon B_{YY}^- + N_-(\epsilon(A^+ + \epsilon B^+), \epsilon(A^- + \epsilon B^-)) - N_0(A^-, \epsilon). \end{aligned} \quad (2.12)$$

Let us study the nonlinear function N_+ as a function of two complex variables $N_+ = N_+(A, B)$. Equations (2.5)–(2.7) imply that

$$m_1 = m_2 + 1, \quad n_1 = n_2 = j - m_2.$$

It follows that $N_+(A, B)$ equals

$$\begin{aligned} & \epsilon^{-3} \sum_{j=1}^{\infty} \sum_{m_2 \leq j} C_{m_2+1}^{2j+1} \cdot C_{m_2}^{2j-m_2} \cdot C_{j-m_2}^{2(j-m_2)} \cdot [(2j+1)!]^{-1} \cdot |A|^{2m_2} \cdot |B|^{2(j-m_2)} (-1)^j A, \\ & = \epsilon^{-3} A \sum_{j=1}^{\infty} \sum_{m_2 \leq j} \frac{1}{[(j-m_2)!]^2} \cdot \frac{1}{m_2!} \cdot \frac{1}{(m_2+1)!} \cdot |A|^{2m_2} \cdot |B|^{2(j-m_2)} (-1)^j. \end{aligned} \quad (2.13)$$

The last sum, denoted by S , is considered for $m = 0$ and $m \geq 1$ separately as

$$\begin{aligned} S &= \sum_{j=1}^{\infty} (-1)^j \frac{1}{(j!)^2} |B|^{2j} + \sum_{m \geq 1} (-1)^m \sum_{j \geq m} \frac{1}{m!} \frac{1}{(m+1)!} \frac{1}{((j-m)!)^2} \cdot |A|^{2m} (-|B|^2)^{j-m} \\ &= \sum_{j=1}^{\infty} (-|B|^2)^j / (j!)^2 + \sum_{m \geq 1} \frac{(-1)^m |A|^{2m}}{m! \cdot (m+1)!} \cdot \sum_{j' \geq 0} \frac{(-|B|^2)^{j'}}{(j')^2}. \end{aligned} \quad (2.14)$$

Recalling section 4 of [9],

$$f(y) \equiv \sum_{m \geq 1} \frac{y^m}{m!(m+1)!} \sim -1 + O((-y)^{-3/4}), \quad y \rightarrow -\infty,$$

we have that

$$\begin{aligned} g(y) &\equiv \sum_{m=1}^{\infty} \frac{y^{m+1}}{m!(m+1)!} \\ &= yf(y) \sim -y + O((-y)^{1/4}), \quad y \rightarrow -\infty, \end{aligned} \quad (2.15)$$

and

$$g'(y) = \sum_{m \geq 1} \frac{y^m}{(m!)^2} \sim -1 + O((-y)^{-3/4}), \quad y \rightarrow -\infty. \quad (2.16)$$

It follows that S is uniformly bounded, and

$$|N_+(A, B)| \leq C_+ \epsilon^{-3} |A|,$$

for a constant C_+ uniformly in A, B . Similarly,

$$|N_-(A, B)| \leq C_- \epsilon^{-3} |B|.$$

Hence,

$$\begin{aligned} |N_+(\epsilon(A^+ + \epsilon B^+), \epsilon(A^- + \epsilon B^-))| &\leq C_+ \epsilon^{-2} |A^+ + \epsilon B^+|, \\ |N_-(\epsilon(A^+ + \epsilon B^+), \epsilon(A^- + \epsilon B^-))| &\leq C_- \epsilon^{-2} |A^- + \epsilon B^-|. \end{aligned} \quad (2.17)$$

Now we show the global well-posedness of system (2.11)–(2.12), where A_{\pm} are globally smooth [9].

Theorem 2.1. *For initial data $(B^+, B^-)|_{\tau=0} \in (H^2(\mathbb{R}^n))^2$, $(B_{\tau}^+, B_{\tau}^-)|_{\tau=0} \in (H^1(\mathbb{R}^n))^2$, the initial value problem of the system (2.11)–(2.12) has a unique global solution $(B^+, B^-) \in C([0, \infty); (H^2(\mathbb{R}^n))^2)$, $(B_{\tau}^+, B_{\tau}^-) \in C([0, \infty); (H^1(\mathbb{R}^n))^2)$, $(B_{\tau\tau}^+, B_{\tau\tau}^-) \in C([0, \infty); (L^2(\mathbb{R}^n))^2)$.*

Proof. We bound $\|(B^+, B^-)\|_2$, and $\|\nabla_{\tau, X_1, Y}(B^+, B^-)\|_2$ for all time. Let us denote the nonlinearities $N_+ - N_0$ in (2.11) by F^+ , and $N_- - N_0$ in (2.12) by F^- . The mass identities are ($\int = \int_{\mathbb{R}^2}$):

$$\frac{d}{d\tau} \left(\int |B^{\pm}|^2 - \frac{\epsilon}{\omega} \operatorname{Im} \int (B^{\pm})^* B_{\tau}^{\pm} \right) = \frac{1}{\omega} \operatorname{Im} \int F^{\pm} (B^{\pm})^*, \quad (2.18)$$

and energy identities are

$$\frac{d}{d\tau} \epsilon \int |B_{\tau}^{\pm} \pm \nu B_{X_1}^{\pm}|^2 + (1 - \nu^2) |B_{X_1}^{\pm}|^2 + |B_Y^{\pm}|^2 = 2 \operatorname{Re} \int F^{\pm} (B_{\tau}^{\pm} \pm B_{X_1}^{\pm})^*. \quad (2.19)$$

Integrating (2.18) over $\tau \in [0, t_1]$ gives

$$\|(B^+, B^-)\|_2^2 - \frac{\epsilon}{\omega} \operatorname{Im} \int (B^+, B^-)^* \cdot (B_\tau^+, B_\tau^-) \leq C_0 + \frac{1}{\omega} \int_0^{t_1} \operatorname{Im} \int (F^+, F^-) \cdot (B^+, B^-)^*, \quad (2.20)$$

where C_0 depends on initial data. Applying the Cauchy-Schwarz inequality and bounds of F^+ to (2.20) yields

$$\begin{aligned} \|(B^+, B^-)\|_2^2(t_1) &\leq C_1 \|(B^+, B^-)_\tau\|_2^2(t_1) + C_0 + C_2 \int_0^{t_1} (\|A^+, A^-\|_2^2 \\ &\quad + \|(B^+, B^-)\|_2^2), \end{aligned} \quad (2.21)$$

where C_1 and C_2 are constants depending on ϵ, ω . Similarly, we obtain from (2.19)

$$\begin{aligned} \|\nabla_{\tau, X_1, Y}(B^+, B^-)\|_2^2(t_1) &\leq C_3 + C_4 \int_0^{t_1} (\|A^+, A^-\|_2^2 + \|(B^+, B^-)\|_2^2 \\ &\quad + \|\nabla_{\tau, X_1}(B^+, B^-)\|_2^2), \end{aligned} \quad (2.22)$$

where C_i s ($i = 3, 4$) are constants depending on ϵ . Multiplying (2.22) by $2C_1$ and adding the resulting inequality to (2.21), we find

$$\|(B^+, B^-)\|_2^2(t_1) + C_1 \|\nabla_{\tau, X_1, Y}(B^+, B^-)\|_2^2(t_1) \leq C_5(t_1) + C_6 \sum_{\pm} \int_0^{t_1} \|(B^\pm, \nabla_{\tau, X_1} B^\pm)\|_2^2, \quad (2.23)$$

where $C_5 = C_5(t_1)$ is an increasing function of $t_1, \forall t_1 > 0$, and depends on $\int_0^{t_1} \|A^\pm\|_2^2(t) dt$; and C_6 is a constant depending on ϵ . Gronwall's inequality and (2.23) imply that for any $t_1 > 0$ $\|(B^\pm, \nabla_{\tau, X_1, Y} B^\pm)\|_2$ are finite. The estimates of higher derivatives are similar. The proof is finished. \square

The asymptotic solutions constructed above render theoretical support for the robustness of colliding pulses observed numerically in the next section.

Let us remark that proving the validity of ansatz (2.2) or its like requires an asymptotic analysis of the singularly perturbed (2+1) nonlinear Schrödinger equations (2.9)–(2.10) for small ϵ , and control of the remainder term R on the time scale $O(\epsilon^{-2})$. The difficulty involved appears to exceed the level of existing analytical estimates. It is also conceivable that the leading order terms of the ansatz (2.2) may be augmented with suitable higher-order terms in the remainder for this purpose.

3. Numerical Experiments

3.1. Numerical Method, Data, and Parameters

We select the initial data on R^2 as

$$u(x, y, 0) = A_0 e^{-0.04(x^2+y^2)} \sin mx, \quad (3.1)$$

$$u_t(x, y, 0) = -\omega A_0 e^{-0.04(x^2+y^2)} \cos mx, \quad (3.2)$$

for the single pulse solution, and

$$u(x, y, 0) = A_0 e^{-0.04((x-15)^2+y^2)} \sin mx + A_0 e^{-0.04((x+15)^2+y^2)} \sin mx, \quad (3.3)$$

$$u_t(x, y, 0) = \omega A_0 e^{-0.04((x-15)^2+y^2)} \cos mx - \omega A_0 e^{-0.04((x+15)^2+y^2)} \cos mx, \quad (3.4)$$

for the axial (head-on) colliding pulse solution. We shall apply a combination of rotations and translations on these data for the other three collision cases. The wave number m equals 2 (unless otherwise noted) to give only a few oscillations under the envelope, and the dispersion relation is $\omega = \omega(m) = \sqrt{1+m^2}$. We use a standard explicit second-order forward time-central space-finite differencing scheme [8], along with a one-sided second-order approximation of the zero Neumann boundary condition at the boundaries of the numerical domain. The method is stable under the stability condition that $\lambda = \frac{k}{h} \leq \frac{1}{\sqrt{2}}$ (h the spatial grid size), which our grid sizes satisfy. The computation is implemented in MATLAB.

In results reported below, an amplitude $A_0 = 1.0$ and $m = 2$ are used for all figures (except where noted). A spatial grid size of $h = 0.1$ and a temporal grid size of $k = 0.05$ are used to satisfy the stability condition. A smaller grid size of $h = 0.075$ was used to verify convergence with no substantial change to the numerical solutions. A movie of the solution was constructed in MATLAB to observe the evolution of the solutions and assist in the qualitative analysis.

3.2. Numerical Results

3.2.1. Single Pulse Solutions. We first look at the single propagating pulses to analyze solution properties without pulse interaction effects. In Figure 1, we plot the solutions for the single pulse solution at three times. The solution propagates from the left to the right boundary of the domain without significant loss of amplitude and is self-supporting (i.e., maintains its shape). This is better observed in Figure 2, which shows the pulse sectional profile along x at $t = 0$ and $t = 45$. Over time, the envelope tends to expand slightly parallel to the x -axis while slightly focusing parallel to the y -axis. We see a wake trailing at a slower velocity than the pulse. Another phenomenon is the “bending” of the pulse envelope over time. The outside edge begins to move at a slower velocity than the centerline of the envelope. In Figure 3, this effect is shown by a top view of the pulse at $t = 0$ and $t = 45$.

3.2.2. Colliding Pulse Solutions.

3.2.3. Axial Collisions. We turn to counterpropagating pulses to see the impact of a direct axial collision. The initial condition (3.3)–(3.4) was used for the axial collision. Figure 4 shows the interaction of two axially colliding pulses. Aside from the direction of propagation, the two initial pulses are identical in amplitude and oscillations under the envelope. The pulses are shown in profile at $t = 0$ and $t = 45$ for comparing the initial and postcollision states. They maintain their overall shapes and amplitudes. Figure 5 shows the pulses at five different times. The pulses approach, collide, pass through each other, and after some time revert back to approximately the original shape and amplitude.

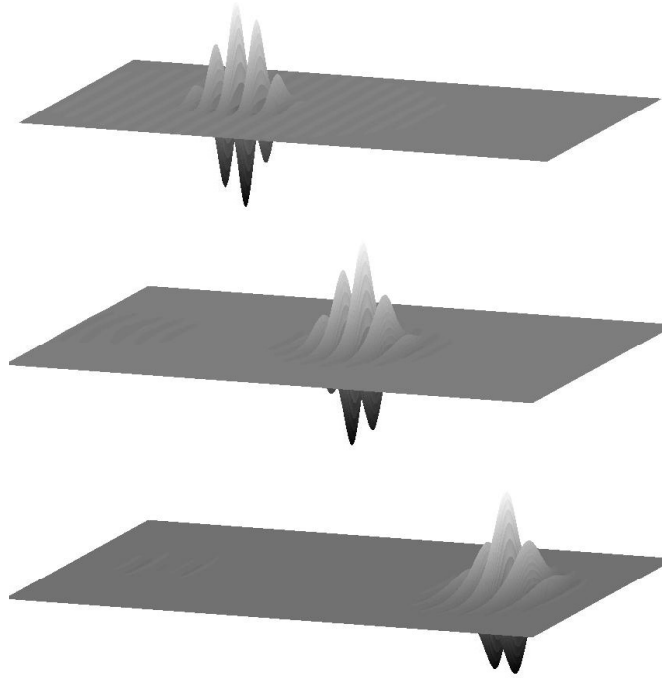


Fig. 1. (2+1) SG single pulse solution, $u(x, y, t)$ for $t = 0, 20, 45$, $x \in [-40, 40]$, and $y \in [-20, 20]$. The pulse propagates from the initial conditions, $u(x, y, 0) = e^{-0.04(x^2+y^2)} \sin 2x$ and $u_t(x, y, 0) = -\sqrt{5}e^{-0.04(x^2+y^2)} \cos 2x$ (top), to the edge of the domain (bottom), retaining its shape.

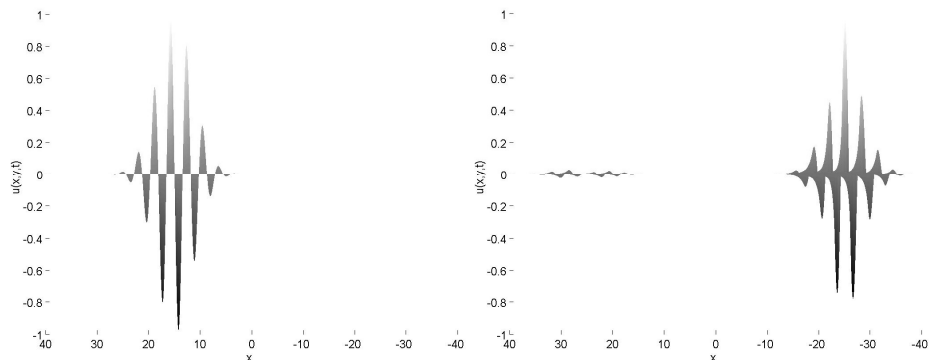


Fig. 2. (2+1) SG single pulse solution, profile view along the x -axis, at $t = 0$ (left) and $t = 45$ (right). This highlights the envelope shape and amplitude. The numerical “wake” can be observed in the right plot. This is the same pulse as in Figure 1.

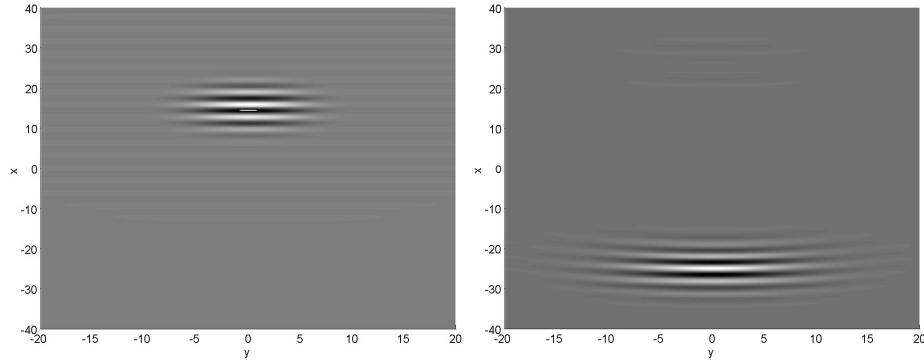


Fig. 3. (2+1) SG single pulse solution, top view. The bending effect can be seen in the changing in the outer edge of the envelope from the initial pulse at $t = 0$ (left) and the propagating pulse at $t = 45$ (right). This is the same pulse as in Figure 1.

As in the previous case, the pulse envelopes undergo a bending phenomenon over time. In the collision cases, however, the bending effect is more pronounced and appears to be a result of the pulse interaction from the collisions.

A comparison of the propagation and collision properties of the (2+1) SG light bullet solutions to those of the full Maxwell system (FMS) in [2] shows many similarities. The light bullet solutions are very stable over time with the appropriate initial data. They are self-supporting (maintaining shape), even after colliding and interacting with other pulses. In the case of the colliding pulses, the FMS light bullets displayed the characteristics of solitons in being essentially unchanged after going through collisions [2]. In the (2+1) SG, we see the same behavior. The pulses interact, separate, and maintain their shapes after undergoing the collisions. Figure 6 shows the stable single pulse and Figure 7 shows the colliding pulses from the FMS [2]. Comparing to Figures 1 and 5,

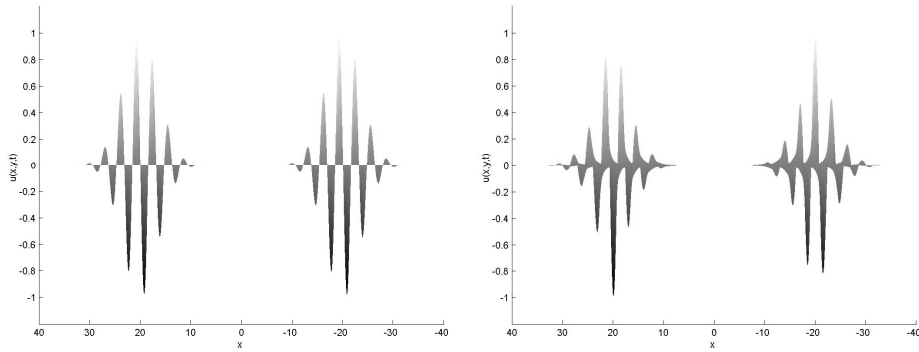


Fig. 4. (2+1) SG axially colliding pulse solution, profile view along x -axis. The initial condition, $u(x, y, 0) = e^{-0.04((x-15)^2+y^2)} \sin 2x + e^{-0.04((x+15)^2+y^2)} \sin 2x$ and $u_t(x, y, 0) = \sqrt{5}e^{-0.04((x-15)^2+y^2)} \cos 2x - \sqrt{5}e^{-0.04((x+15)^2+y^2)} \cos 2x$, at $t = 0$ (left) consists of two pulses, propagating in different directions which pass through each other and continue moving at $t = 45$ (right). They maintain much of their original shapes after collision.

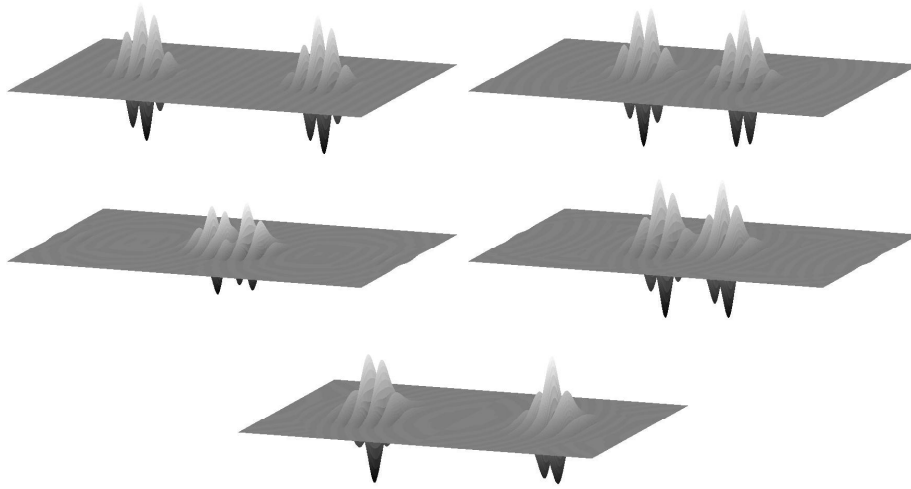


Fig. 5. (2+1) SG axially colliding pulse solution. The pulses are shown at five discrete times ($t = 0, 10, 20, 30, 45$) starting at $t = 0$ (upper left) and proceeding left to right and down until $t = 45$ at the bottom. The initial conditions are identical to Figure 4.

we see that the FMS pulses are qualitatively the same as the SG pulses. We will make further comparisons later in the paper.

3.2.4. 90° and 120° Collisions. We also examined the dynamics of pulses colliding at different angles. We translated and rotated pulses in the initial condition (3.4) so that the pulses would collide at angles of 90° and 120° to see the impact of a collision at each angle. Aside from a translation and rotation, the two initial pulses are identical. In

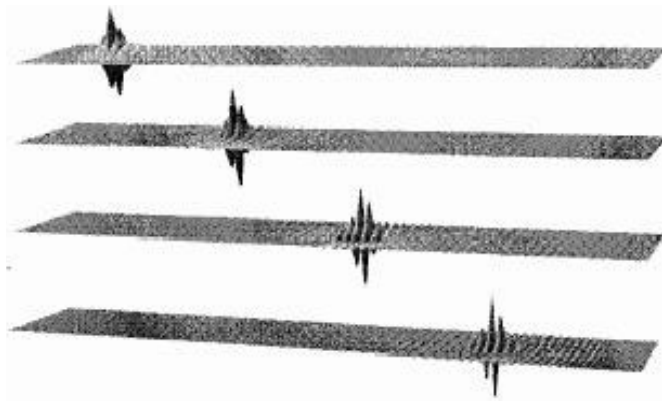


Fig. 6. Maxwell simulations for single pulse. “Electric field of a pulse undergoing dispersion, diffraction, and nonlinear refraction after 155 fs, 310 fs, and 620 fs of propagation. Initial electric-field amplitude, $E_0 = 2.9 \times 10^{10}$ V/m; initial pulse width, $0.9 \mu\text{m}$ (FWHM); initial pulse duration, 18 fs (FWHM); pulse propagation distance, 28 Rayleigh ranges” [2].

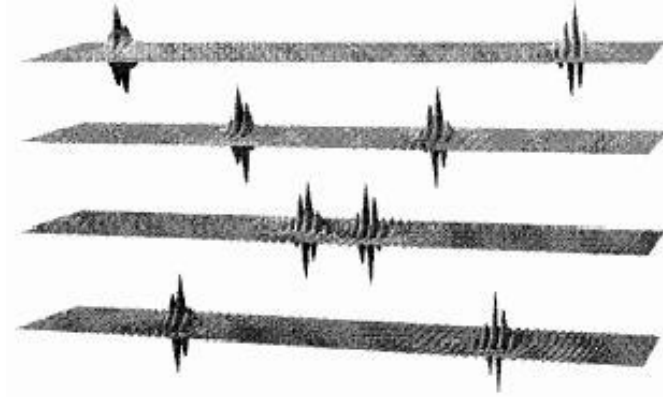


Fig. 7. Maxwell simulations for colliding pulses. “Electric field of two counterpropagating pulses after 155 fs, 465 fs, and 620 fs of propagation.” [2] The initial pulse parameters are given in Figure 6.

Figure 8, we see the evolution of two pulses colliding at a 90° angle. Figure 9 shows the evolution of two pulses colliding at a 120° angle. In both cases, the pulses collide, interact, and then move through each other as in the axial collision case. We also see bending of the envelope after the collision; the outside edge of the envelope appears to be moving at a slightly slower velocity than the centerline. There is no change in the direction of propagation; each pulse continues to move along the same path as before the collision. We observed the same properties in the 120° collision case as we did in the 90° collision case.

3.2.5. Effects of Changing Initial Pulse Parameters. For most of the simulations, we used $A = 1.0$ for the amplitude and $m = 2$ to regulate the number of oscillations under the envelope in the initial pulse. We varied these parameters in the traveling pulse and axially colliding pulse case to observe the results. We used different values of A_0 , while keeping all other values constant, to observe the effect of a change of amplitude in the single pulse solutions. For values $A_0 \in [0.5, 1.5]$, the only observed change was in the amplitude (as expected). When a value of $A_0 < 0.5$ was used, the pulses spread. With values $A_0 > 1.5$, the solutions destabilize and the envelope breaks down in time. In Figure 10, amplitudes of $A_0 = 0.3$ and 2.5 were used, and we plotted u as a function of x , at $y = 0$ and $t = 0, 20, 45$. The solutions disperse with time when $A_0 = 0.3$. At an amplitude of $A_0 = 2.5$, the pulse envelope gradually disappears in time. Solutions were also observed for $A_0 = 1.6, 1.8, 2.0$. A steady increase in the solution expansion and breakdown of the envelopes of the pulses were observed when the amplitude was increased above $A_0 = 1.5$.

We also looked at the effect of increasing the number of oscillations under the envelope. For $m = 5$, we noticed stable pulse propagation and collision as well. Figure 11 shows the solution profiles along the x -axis for both the single pulse and the axially colliding pulses.

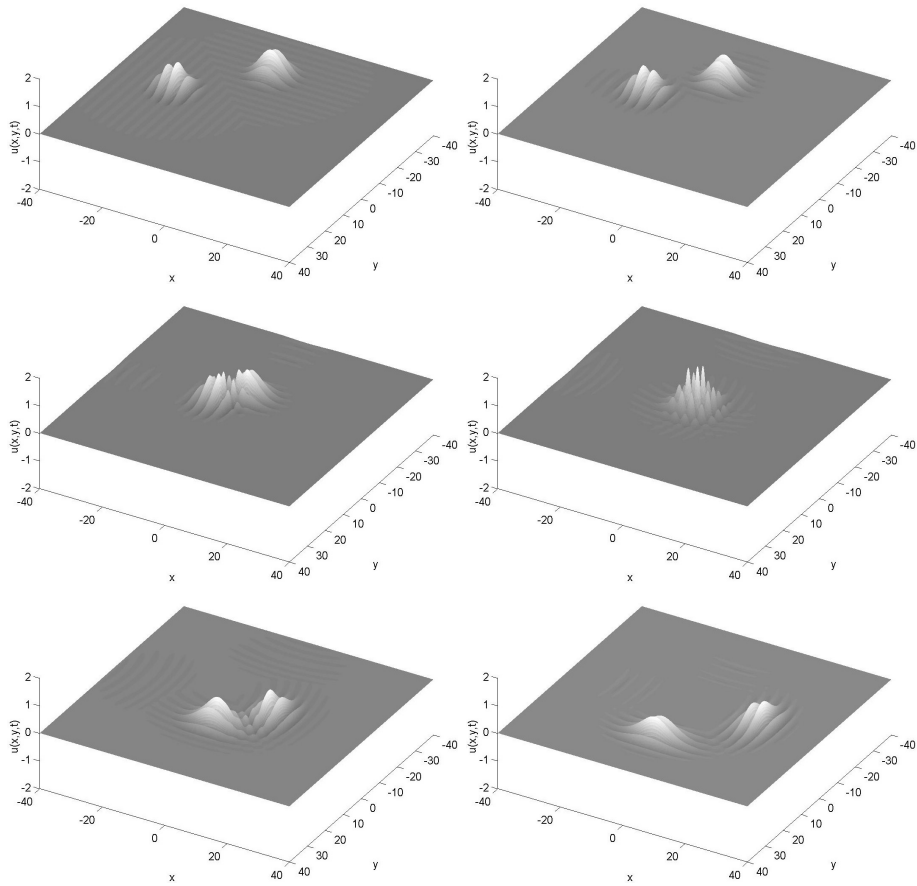


Fig. 8. (2+1) SG colliding pulse solution (90° collision angle), $t = 0, 5, 15, 25, 35, 45$. The initial conditions (same as in Figure 5 except with a translation and 90° rotation of one pulse) at $t = 0$ (top left) consist of two pulses, propagating on perpendicular axes which pass through each other and continue moving at $t = 45$ (bottom right; time increases from left to right and down). The pulses collide, interact, and continue to propagate along the original axes, maintaining their shape.

Finally, in the single moving pulse case, we looked at the effect of increasing the wave number and amplitude simultaneously. We used $m = 5$ and looked at solutions with initial amplitudes $A_0 = 1.5, 2.5,$ and 3.5 . In Figure 12, we plotted u as a function of x at $y = 0$ and $t = 0, 20, 45$ for all three amplitudes. We see that the breakdown of the envelope is much weaker with the increase in m .

4. Conclusions

The asymptotics of a pair of counterpropagating solutions to the SG equation is constructed in more than one space dimension. The asymptotic equations are well-posed for

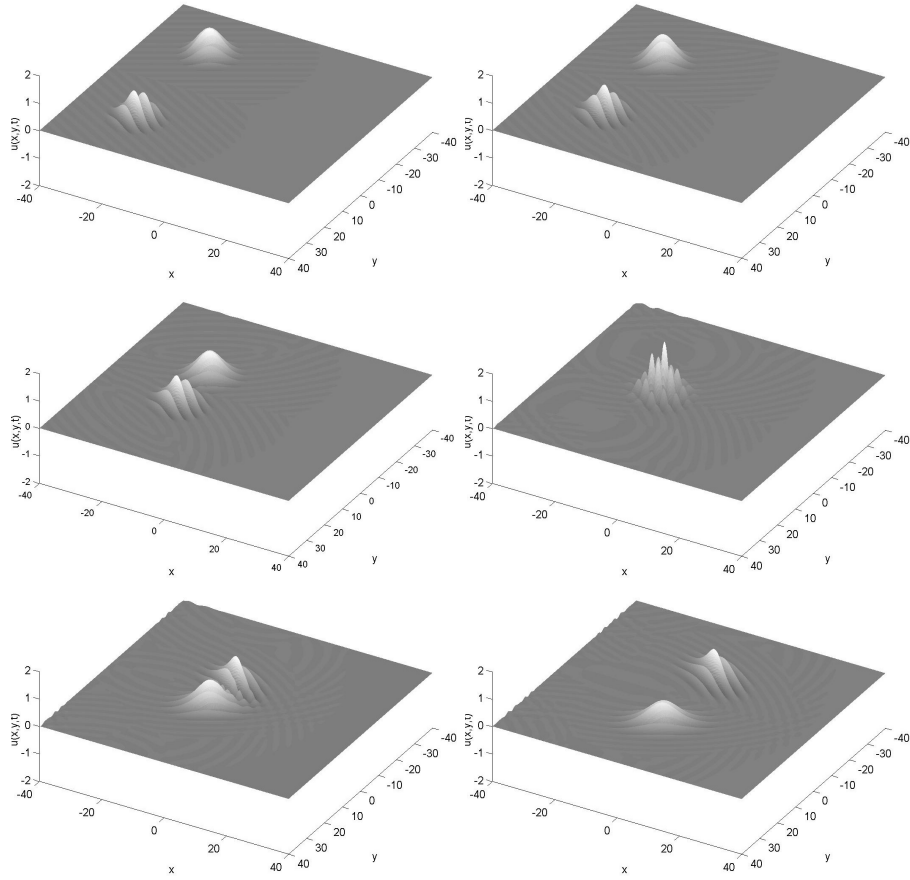


Fig. 9. (2+1) SG colliding pulse solution (120° collision angle). The initial conditions consist of two pulses, propagating on axes intersecting at 120° , which pass through each other and continue moving at $t = 45$ (bottom right; time increases from left to right and down). The pulses collide, interact, and continue to propagate along the original axes, maintaining their shape.

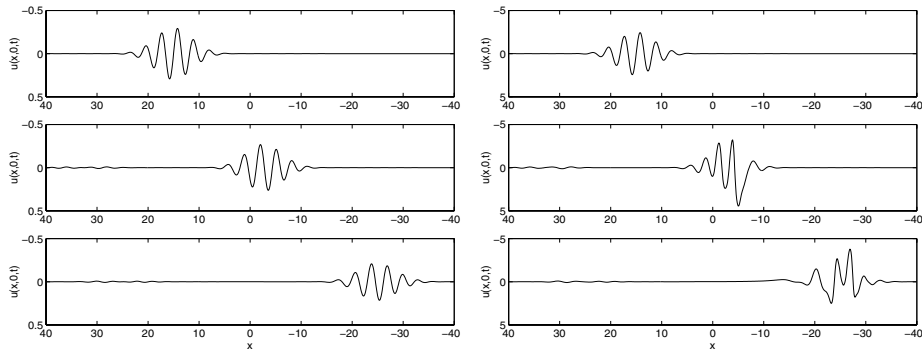


Fig. 10. Effects of changing amplitude: (2+1) SG single pulse solution $u(x, 0, t)$, $A_0 = 0.3$ (left) and $A_0 = 2.5$ (right), both for $t = 0, 20, 45$ (from top to bottom).

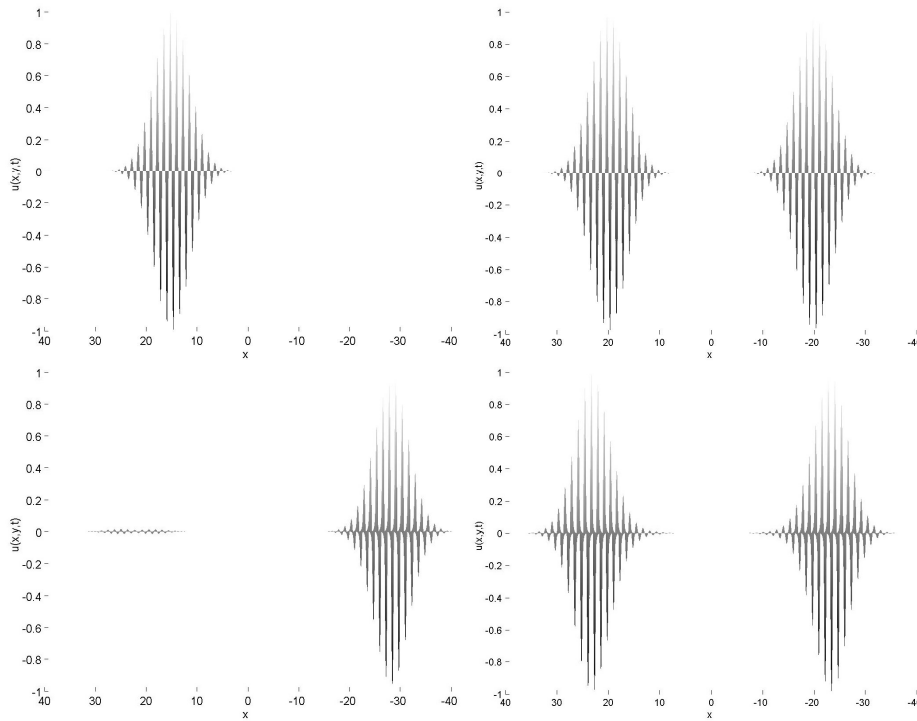


Fig. 11. (2+1) SG single pulse solution (left) and axially colliding pulses (right), $u(x, y, t)$, $m = 5$, profile view along x axis, $t = 0$ (top) and $t = 45$ (bottom).

all time. The asymptotic theory serves as a theoretical basis for numerically observed robust propagation and interaction of spatially localized pulses. The pulse solutions are self-supporting (maintaining shape), even after colliding and interacting with other pulses at different angles. In a simulation of the cubic Maxwell system [2], similar pulses are self-supporting in a given energy range, just like (2+1)SG pulses which require the amplitude of the initial pulse to lie in a specific range. Comparing Figure 7, the Maxwell light bullets, with Figures 1 and 5 suggests qualitative agreement.

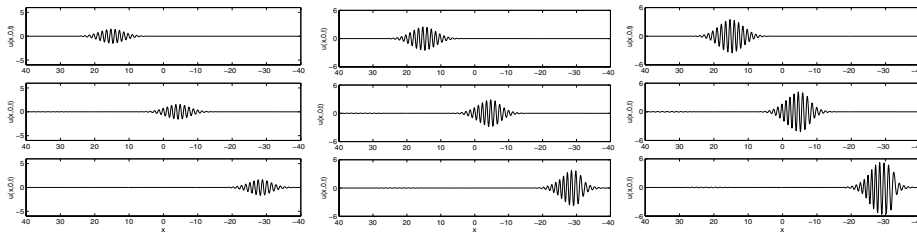


Fig. 12. (2+1) SG single pulse solution, $u(x, 0, t)$, $m = 5$, $A_0 = 1.5$ (left), 2.5 (middle) and 3.5 (right), for $t = 0, 20, 45$ (from top to bottom).

We leave as future work the quantitative analysis of the closeness of the asymptotic solutions to exact SG solutions.

Acknowledgments.

The work was partially supported by ARO and NSF grants to J. X. at the Institute of Computational and Engineering Sciences (ICES), University of Texas at Austin.

References

- [1] M. Ablowitz, H. Segur, *Solitons and the Inverse Scattering Transform*, SIAM Studies in Applied Mathematics, Philadelphia, 1981.
- [2] P. Goorjian, Y. Silberberg, *Numerical simulations of light bullets using the full-vector time-dependent nonlinear Maxwell equations*, Journal of the Optical Society of America B (Optical Physics) 14, no. 11 (1997), pp. 3253–3260.
- [3] R. McLeod, K. Wagner, S. Blair, *(3+1)-dimensional optical soliton dragging logic*, Physical Review A 52, no. 4 (1995), pp. 3254–3278.
- [4] A. Minzoni, N. Smyth, A. Worthy, *Pulse evolution for a two-dimensional Sine-Gordon equation*, Physica D 159 (2001), pp. 101–123.
- [5] A. Minzoni, N. Smyth, A. Worthy, *Evolution of two-dimensional standing and traveling breather solutions for the Sine-Gordon equation*, Physica D 189 (2004), pp. 167–187.
- [6] A. Newell, J. Moloney, *Nonlinear Optics*, Addison-Wesley, Redwood City, CA, 1991.
- [7] R. D. Pierce, C. E. Wayne, *On the validity of mean-field amplitude equations for counter-propagating wavetrains*, Nonlinearity 8 (1995), pp. 769–779.
- [8] J. Strikwerda, *Finite Difference Schemes and PDE*, Wadsworth and Brooks, Cole Adv. Books and Software, 1989.
- [9] J. Xin, *Modeling light bullets with the two-dimensional sine-Gordon equation*, Physica D, 135 (2000), pp. 345–368.
- [10] J. Xin, J.-M. Yuan, *A numerical study of a perturbed critical nonlinear Schrödinger equation arising from the (2+1) sine-Gordon equation*, in preparation.